

Imaging properties of planar-integrated micro-optics

Markus Testorf

Department of Electrical and Computer Engineering, University of Massachusetts–Lowell, One University Avenue, Lowell, Massachusetts 01854

Jürgen Jahns

FernUniversität Hagen, Optische Nachrichtentechnik, Feithstrasse 140, 58084 Hagen, Germany

Received July 13, 1998; revised manuscript received October 23, 1998; accepted November 2, 1998

The properties of planar-integrated imaging systems are studied on the basis of algebraic ray tracing. A third-order approximation yields analytical expressions for ray aberrations in the image plane. Ray aberrations are compared with the diffraction-limited spot size to estimate optimum system performance from the minimum of the second moment of the point-spread function. We use as a figure of merit the space–bandwidth product of the planar imaging setups. The investigation is restricted to imaging systems consisting of three optical elements. © 1999 Optical Society of America [S0740-3232(99)00605-5]

OCIS codes: 350.3950, 110.0110, 080.1010.

1. INTRODUCTION

Optical interconnection systems based on free-space optics can provide a large number of high-bandwidth channels. The planar integration of free-space optics¹ is a concept designed for matching the advantages of optics with the needs of integrated electronic circuits. In this context, planar integration means the arrangement of optical elements on the surface of a thick transparent substrate. The light signal travels within the substrate from one element to the next one, along a folded path reflected at the surfaces of the substrate.

An important basic operation of free-space optics is imaging. Typical applications are optical relay systems and interconnects. It has already been demonstrated that imaging systems can be realized as planar-integrated setups.² In planar optics the system properties depend on the oblique orientation of the optical axis.^{3,4} It is known that for optical systems, which are not rotationally symmetric, additional aberrations occur, which are not present for the corresponding rotationally symmetric system.⁵ It has already been shown that, for a single-lens system, these aberrations reduce the number of points that can be resolved by the planar imaging setup.⁶

Here we address in more detail the problem of planar optical imaging to characterize the imaging performance quantitatively. To this end, we evaluate the properties of a system consisting of three diffractive optical elements (Fig. 1) in terms of a third-order aberration theory. We investigate as particular examples a single-lens system and a $4f$ system. We show that most third-order aberrations can be compensated in a planar $4f$ system. From analytic expressions of the ray aberrations we determine the imaging performance of both planar optical systems. We use as a figure of merit the number of resolved image

points, i.e., the space–bandwidth product (SBP) of the optical system.

Planar optics can be implemented with diffractive and refractive micro-optical elements. For practical purposes and technological reasons, mostly diffractive optics has been used thus far. This also provides a high flexibility for designing elements with a desired response. Note, however, that the use of refractive elements for planar optics was considered recently.^{7,8}

Here we consider systems based on thin phase-only elements. We assume that any kind of slowly varying phase retardation profile can be implemented. Although, for monochromatic illumination, this can be realized more easily with diffractive optics, the scope of our investigation is not limited to any particular technology. A further condition that we impose is that the system not contain stops at planes intermediate to the optical elements that are located at the surfaces of the substrate. Although stops can be implemented in planar optics by use of suitable absorbing layers, they are typically located at these surfaces as well and cannot be placed arbitrarily within the substrate to improve the aberration characteristics. Therefore we consider only the finite aperture of the optical elements.

Our study has three aims. First, we outline a ray-tracing method that can be used to characterize planar optical systems. The computation scheme is based on symbolic computer algebra. Computer algebra was recently proposed as an attractive alternative to numerical ray-tracing methods for solving lens design problems.⁹ The scheme that we use is applicable to a wide class of systems and is well suited for analyzing other planar optical setups as well. Its scalability is limited only by the speed and the memory limitations of the computer sys-

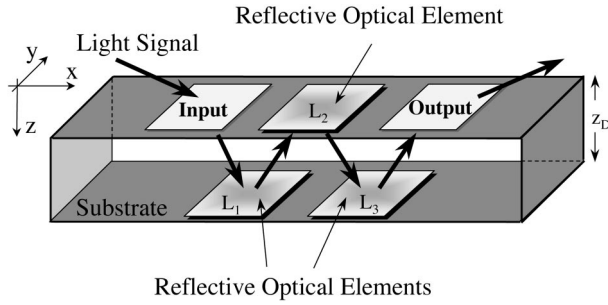


Fig. 1. Planar-integrated optical imaging systems with three diffractive optical elements.

tem. Second, we characterize planar imaging systems and their imaging properties. Third, we illustrate the way in which the demand for optimum imaging performance determines the system parameters of the planar setup.

To achieve these aims, in Section 2 we summarize the ray-tracing equations for planar-integrated optical systems. Then, in Section 3, we give the motivation for the choice of the planar optical systems that we discuss. In addition, we briefly summarize the first-order properties. In Section 4 we characterize the systems in terms of third-order aberrations. Finally, in Section 5, we compare the ray aberrations to the diffraction-limited performance of the imaging system, taking into account the geometry constraints of planar-integrated optics. This allows us to estimate the SBP of planar-integrated imaging systems.

2. MATHEMATICAL MODEL AND NOTATION

Ray tracing of light signals through optical systems has been studied extensively in the past. For our investigation of planar-integrated imaging systems, we in essence adapt a method described in Ref. 10 for rotationally symmetric systems. It allows the analysis of arbitrarily composed optical systems by chaining of the ray transfer functions of free-space and optical elements.

Figure 2 illustrates the coordinate system that we are using. We consider the unfolded planar-integrated setup, where tilted optical elements are located in planes $x-y$ along the optical axis s . We assume the z axis to lie in the $x'-s$ plane. Ray tracing is performed in the Cartesian coordinate system $x'-y-s$. An optical ray is specified by its lateral space coordinates $\mathbf{r} = (x', y)$ and its propagation direction $\mathbf{u} = (v, w)$. The directional cosines v and w are the projections of the unit length propagation vector onto the $x'-y$ plane.

For free-space propagation the initial propagation direction \mathbf{u}_{in} is preserved while the ray propagates from the input plane s to the output plane $s + \Delta s$; hence we can write, for the output propagation direction,

$$v_{out} = v_{in}, \quad w_{out} = w_{in}. \quad (1)$$

Free-space propagation results in a lateral shift of the ray position. Making use of the unit length of the propagation vector, i.e., $|\mathbf{u}| = 1$, we obtain the space coordinates of the output ray:

$$x'_{out} = x'_{in} + \Delta s_p \frac{v_{in}}{(1 - v_{in}^2 - w_{in}^2)^{1/2}},$$

$$y_{out} = y_{in} + \Delta s_p \frac{w_{in}}{(1 - v_{in}^2 - w_{in}^2)^{1/2}}. \quad (2)$$

Equations (2) are the exact equations to describe propagation in free space. The tilt of the optical elements makes Δs_p a function of the propagation vector \mathbf{u} and the tilt angle ϑ :

$$\Delta s_p = \Delta s \left(1 - \frac{v \tan \vartheta}{\sqrt{1 - v^2 - w^2}} \right)^{-1}. \quad (3)$$

It is this dependency of Δs_p that distinguishes the imaging properties of planar systems from their rotationally symmetric counterparts.

The change of the propagation direction of an optical ray as caused by an optical element, either diffractive or refractive, is given by^{11,12}

$$\mathbf{u}_{out} = \mathbf{u}_{in} + \mathbf{k}_g(\mathbf{r}), \quad (4)$$

where $\mathbf{k}_g(\mathbf{r})$ is the slowly varying local spatial frequency of the element. For a refractive element this refers to the gradient of the phase retardation, while for a diffractive element $\mathbf{k}_g(\mathbf{r})$ is associated with the local grating vector.

For our investigation we assume phase-only elements, for which the phase distribution ϕ is described by a power series

$$\phi(x', y) = 2\pi \sum_m \sum_n a_{mn} x'^m y^n. \quad (5)$$

Equation (5) defines the phase distribution in $x'-y$ coordinates. The equivalent expression for the $x-y$ plane in which the element is located can be obtained by substitution of $x' = x \cos \vartheta$. The local spatial-frequency vector is given by the gradient of the phase function

$$\mathbf{k}(\mathbf{r}) = \frac{1}{2\pi} \nabla \phi(\mathbf{r}), \quad (6)$$

and we obtain the following expressions for the change of the propagation direction:

$$v_{out} = v_{in} + \sum_m \sum_n m a_{mn} x'^{m-1} y^n, \quad (7)$$

$$w_{out} = w_{in} + \sum_m \sum_n n a_{mn} x'^m y^{n-1}. \quad (8)$$

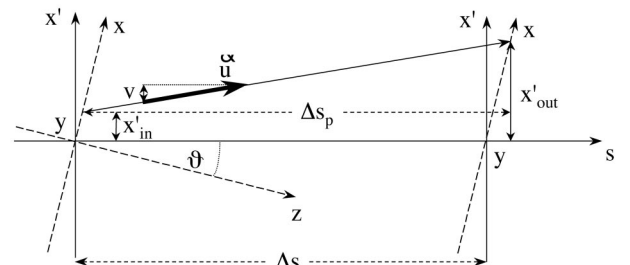


Fig. 2. Coordinate system used for ray tracing in planar-integrated systems: unfolded geometry.

The use of thin optical elements ensures that

$$x'_{\text{out}} = x'_{\text{in}}, \quad y_{\text{out}} = y_{\text{in}}. \quad (9)$$

Equations (1)–(9) relate the input and the output coordinates of the rays in the planar integrated system. Starting with the input location and the propagation direction of the ray, we can obtain the output coordinates of the entire system by taking the output coordinates of each element or propagation step in free space as input for the next element or propagation step. Obviously, even for simple systems, the resulting expressions become very complex. Therefore, as a final step, we calculate the Taylor expansion of the output coordinates with respect to ray location and direction in the input plane.

The first-order coefficients correspond to Gaussian optics, while higher-order terms contain information about aberrations. Aberrations are expressed as deviations of the output ray location from the Gaussian image point, given as a function of input location and direction. For this investigation we consider only coefficients up to the third order in the input coordinates. Note that the calculated Taylor coefficients do not directly correspond to the classical Seidel aberrations, which are obtained from a power series of the Gaussian image point and the ray location in the exit pupil. There is, however, a unique relation between the coefficients of our notation and the Seidel aberrations.

The computation of aberration coefficients, including the Taylor expansion, can be conveniently performed with the help of programs for symbolic computation. The computation scheme outlined thus far allows a straightforward analysis of rather complex systems. The analytic expressions obtained from this procedure provide a much better insight into the properties of the planar optical system than can be obtained from a numerical ray trace.

The algebraic computation scheme can be applied to the same class of problems as conventional aberration theory. The expansion coefficients describe the aberrations of a paraxial wave field, and a large number of coefficients have to be calculated to account for rays with large propagation angles. The accuracy of a particular

calculation can be estimated with the help of expansion coefficients of the next higher order. For the systems that are investigated in this study, we also compared the overall system performance discussed in Section 5 with numerical ray-tracing calculations. The relative deviation from the results obtained with a third-order approximation was determined to be always smaller than a few percent.

For our investigation we had access to a MAPLE V (Release 3) software package. On a Pentium PC with 200-MHz CPU clock frequency the computation of a three-element system takes less than 15 s and occupies approximately 16 Mbytes of physical memory. Execution speed and required memory are only moderately dependent on the number of calculated Taylor coefficients but increase significantly with each additional element. Although we did not explore in detail the complexity of our algorithm, we generally found that both execution time and allocated memory increase by approximately 50% for each additional element. Therefore, for very complex systems, it is necessary to calculate the Taylor expansion at several intermediate planes. The polynomial expansion preserves the complexity of the algebraic expression, and hence the memory load remains almost constant, while the execution time generally increases linearly with the number of optical elements.

3. PLANAR OPTICAL SYSTEM CONSISTING OF THREE ELEMENTS

For our discussion we concentrate on the specific properties of planar-integrated systems as compared with conventional optics. We assume that the optical system is composed of no more than three diffractive optical elements. For rotationally symmetric systems, three aspheric surfaces are sufficient to compensate for third-order aberrations.¹³ The presence of any third-order aberration in the corresponding planar-integrated setup characterizes the difference between conventional optics and planar-integrated optics. Figure 3(a) shows the basic planar system that we are analyzing. The input

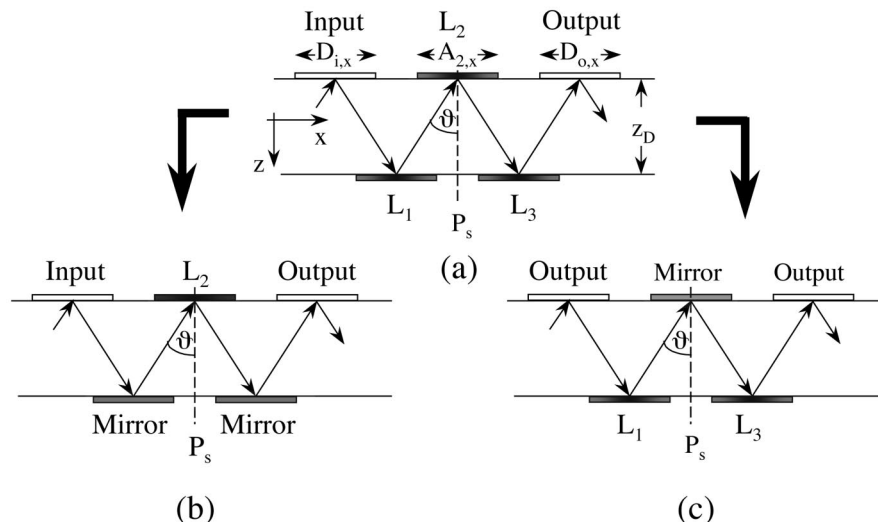


Fig. 3. Examples of imaging systems that can be derived from (a) the three-element setup; (b) single-lens system, (c) $4f$ system.

plane D_i is imaged to the output plane D_o by means of three elements separated by equal propagation steps. From this setup two particular cases can be identified: the single-lens system [Fig. 3(b)], and the $4f$ system [Fig. 3(c)]. We assume as an additional constraint that the system is symmetric with respect to the line P_s . This means that imaging is performed with unit magnification. With some modifications the folded geometry of Figs. 3(a) and 3(c) reflects the symmetry of the Offner projection system¹⁴ and the Fastie–Ebert monochromator.¹⁵ Both systems have a folded geometry similar to planar-integrated optics. In addition, both systems are known to perform imaging with small aberrations, which was the initial motivation for our choice of the planar imaging system.

The first-order imaging properties can be calculated from Eqs. (1)–(9) by consideration of only terms with a linear dependence on the input coordinates. For ideal imagery the location of the output ray \mathbf{r}_{out} has to be independent of the propagation direction of the input ray \mathbf{u}_{in} . This yields two cases, namely, $\mathbf{r}_{\text{out}} = \mathbf{r}_{\text{in}}$, and $\mathbf{r}_{\text{out}} = -\mathbf{r}_{\text{in}}$; here we consider only the second case.

The three lenses L_i in Fig. 3 are characterized by the coefficients $a_{i,20}$ and $a_{i,02}$ in Eq. (5). Because of the symmetry of the system, L_1 and L_3 are equal, i.e., $a_{1,02} = a_{3,02}$, and $a_{1,20} = a_{3,20}$. The remaining free coefficients are interrelated, and we obtain

$$a_{1,mn} = -\frac{\cos \vartheta \cos \vartheta + 2a_{2,mn}z_D}{2z_D \cos \vartheta + a_{2,mn}z_D}, \quad (10)$$

with $mn = 02, 20$. Equation (10) offers the possibility of distributing the focusing power freely between elements. This is important if the minimum feature size of the fabrication process does not allow incorporation of all the focusing power into only one or two of the optical elements. The coefficients in Eq. (10) describe the phase distribution in the rectangular coordinate system that we use for ray tracing. However, the focal length of a lens is usually expressed as the inverse curvature of a parabolic phase function in the plane x – y , where the element is located. According to our definitions, we find a different focal distance for x and y :

$$f_x = -\frac{1}{2a_{20} \cos^2 \vartheta}, \quad f_y = -\frac{1}{2a_{02}}. \quad (11)$$

This reflects the astigmatism introduced, by the oblique propagation direction of light, with respect to the z axis.^{3,4}

In Eq. (10) we recognize the single-lens system for $a_{1,20} = a_{1,02} = 0$ and the $4f$ system for $a_{2,20} = a_{2,02} = 0$. In both systems the remaining coefficients correspond to a focal distance of

$$f_x = \frac{z_D}{\cos^3 \vartheta}, \quad f_y = \frac{z_D}{\cos \vartheta}. \quad (12)$$

4. ABERRATIONS CAUSED BY THE OBLIQUITY OF THE OPTICAL AXIS

Within the first-order approximation all planar systems mentioned thus far are equally well suited to image the input plane to the output plane. To notice any difference

we have to investigate the third-order properties. The number of free lens parameters is determined by the symmetry of the planar system, i.e., $a_{i,mn} = 0$ when either n or m is an odd integer value. For the remaining coefficients of L_1 and L_3 we again assume that $a_{1,mn} = a_{3,mn}$.

Obviously, other choices of the lens coefficients provide the freedom to balance different types of aberration. This, however, is not a specific problem of planar optics. Our choice of a symmetric system allows us to concentrate on the differences between planar systems and rotational symmetric systems, which is our main concern.

As mentioned above, aberrations are characterized by the ray deviation $\Delta x'$ and Δy from the Gaussian image point, expressed as

$$\Delta x' = \sum_{p,q} X_{pq} p q + \sum_{o,p,q} X_{opq} o p q, \quad (13)$$

$$\Delta y = \sum_{p,q} Y_{pq} p q + \sum_{o,p,q} Y_{opq} o p q, \quad (14)$$

where $p, q = x', y, v, w$. Because of the obliquity of the optical axis, Eqs. (13) and (14) also include second-order contributions. Note that these second-order terms are not unique to planar-integrated optics. It has been shown before that these terms can occur in any nonrotationally symmetric system.⁵ Recently, it was shown that these contributions cause additional wave aberrations in a single-lens system, which significantly decreases the resolution in a single-lens imaging system.⁶

For the third-order approximation we find aberrations of almost all types. The aberration coefficients that we obtained from the ray-tracing procedure are listed in Appendix A. As second-order contributions $\Delta x'^{(2)}$ we obtain

$$\begin{aligned} \Delta x'^{(2)} &= X_{x'x'} x'^2 + X_{x'v} x' v', \\ \Delta y^{(2)} &= Y_{x'y} x' y + Y_{x'w} x' w + Y_{yv} y v. \end{aligned} \quad (15)$$

The set of nonzero second-order terms reflects the orientation of the optical axis within the x – z plane. All terms of second order depend on $\sin \vartheta$; i.e., these terms vanish for rotationally symmetric systems. However, they become dominant for large angles ϑ .

To investigate the significance of the second-order aberrations we calculated the spot array pattern in the output plane of the single-lens system separately for second- and third-order aberrations [Figs. 4(a) and 4(b), respectively]. We assume a substrate thickness of $z_D = 6$ mm, a propagation angle of $\vartheta = 15^\circ$, and a lens f -number of $f = 10$, which are realistic values for planar optics. Input and output field have a lateral extension of $500 \mu\text{m}$ in each direction. The simulations given in Fig. 4 were performed for a parabolic lens shape.

Figure 4 illustrates that the second-order terms have the greatest effect on image points with a large distance from the optical axis, while the response of the third-order contributions are similar for all points. Hence, for most practical applications, the resolution of the system is limited by the second-order aberrations. Consequently, any design of a planar imaging system should be aimed at avoiding these aberrations.

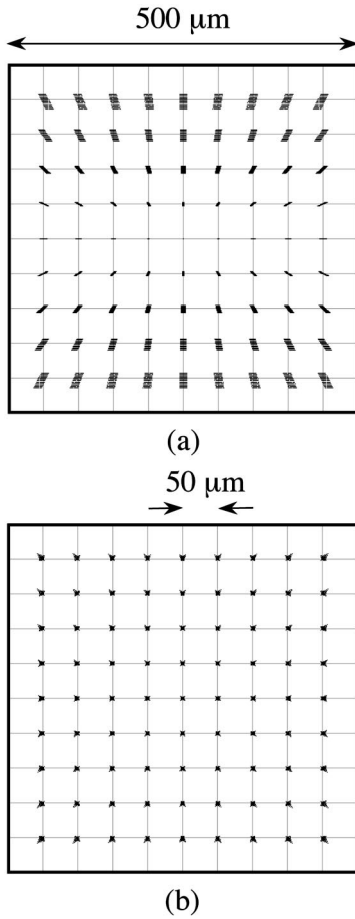


Fig. 4. Spot array patterns of object points in the image plane of the single-lens system assuming a parabolic lens: (a) second-order aberrations, (b) third-order aberrations.

A significant improvement as compared with the single-lens system can be achieved with the $4f$ system. It automatically compensates for all second-order contributions, leaving only ten coefficients of third order (see Appendix B). A further improvement is possible with a third element, L_2 in Fig. 3(a), located in the Fourier plane of the $4f$ system. This element acts as a correction plate for aberrations. Then the third-order terms X_{vvv} , $X_{x'x'v}$, Y_{www} , and Y_{yyw} can be eliminated by a proper choice of $a_{1,40}$, $a_{2,40}$, $a_{1,04}$, and $a_{2,04}$ without affecting any other type of aberration.

The three remaining free lens parameters can compensate for up to three of the six remaining aberration terms. For instance, $\Delta x = 0$ can be achieved, which leaves the terms Y_{vvw} , $Y_{x'x'w}$, and $Y_{x'yv}$. Thus the three-element system provides a significant improvement of the imaging characteristic. However, as for the single-lens system, the obliquity of the optical axis causes additional aberrations. This can be appreciated by inspection of the remaining contribution listed in Appendix B. For $\vartheta = 0$ all aberrations of third order can be compensated.

5. RAY ABERRATIONS AND DIFFRACTION-LIMITED SPOT SIZE

Thus far, we have discussed only the ray optical properties of planar imaging systems. However, to estimate the

imaging performance, we must compare ray aberrations with the diffraction-limited performance of the system. We investigate as a figure of merit the number of points that can be resolved by the imaging system, also referred to as the SBP:

$$\text{SBP} = \frac{D_{x'} D_y}{\delta x' \delta y}, \quad (16)$$

where $D_{x'}$ and D_y are the lateral extensions of the input or the output area and $\delta x'$ and δy is the image spot size in x' and y , respectively.

For the following discussion we relate the spot size to the second-order moment of the point-spread function (PSF). Then we can estimate the spot size with twice the variance of the PSF:

$$\delta x' = 2\sqrt{m_{x'}}, \quad \delta y = 2\sqrt{m_y}, \quad (17)$$

with $m_{x'}$ and m_y being the second moments of the PSF in x' and y .

The PSF of the combined effects of diffraction and aberration can be estimated from a theorem of Baraket¹⁶ and Linfoot.¹⁷ According to this theorem, the second moment of the PSF is the sum of the second moment of the diffraction-limited PSF m_d and the second moment of the aberration blur m_r . Optimum imaging conditions are obtained for a minimum of the joint moments

$$m = m_d + m_r. \quad (18)$$

For the diffraction-limited PSF of a rectangular exit pupil, it is possible to estimate that¹⁶

$$m_d = m_{d,x'} + m_{d,y} = 2 \left(\frac{\delta x'_{dl}}{\pi} \right)^2 + 2 \left(\frac{\delta y_{dl}}{2\pi} \right)^2, \quad (19)$$

where $\delta x'_{dl}$ and δy_{dl} are the distances from the center maximum to the first zeros of the PSF in the x' and the y directions, respectively. For a rectangular exit pupil these distances can be calculated from

$$\delta x'_{dl} = \frac{\lambda \Delta s}{A_{i,x'}}, \quad \delta y_{dl} = \frac{\lambda \Delta s}{A_{i,y}}, \quad (20)$$

where Δs is the propagation distance between the exit pupil A_i of the system and the image plane. For the single-lens system it is $A_i = A_2$, where A_2 is the aperture of the lens L_2 . For the $4f$ system we again assume symmetry, i.e., $A_i = A_1 = A_3$.

The folded geometry of planar-integrated optics (Fig. 1) implies an upper bound for the size of lens apertures and input and image planes. In the x' direction this size must be smaller than the lateral shift of the light signal caused by the tilted optical axis. In the $x'-y$ coordinate system this is written as⁴

$$A_{i,x'} \leq 2z_D \sin \vartheta. \quad (21)$$

There is no similar constraint for the y coordinate. In practice, however, the aperture size in y is also limited by the fabrication technology, and it is reasonable to assume that $A_{i,y} = A_{i,x}$ and $D_{x'} = D_y$. To avoid vignetting, we further choose $D = A_2/2$ for the single-lens system and $D = A_2 = A_1/2$ for the $4f$ system.

The second moment of the aberrations m_r can be calculated from the lateral ray aberrations¹⁷:

$$m_r = m_{r,x'} + m_{r,y} = \frac{\int_{v_{\min}}^{v_{\max}} \int_{w_{\min}}^{w_{\max}} (\Delta x'^2 + \Delta y^2) dv dw}{(v_{\max} - v_{\min})(w_{\max} - w_{\min})}. \tag{22}$$

The integration limits correspond to the cone of propagation angles that is passing the optical system. v_{\min} , v_{\max} , w_{\min} , and w_{\max} , as well as $\Delta x'$ and Δy , are functions of the input coordinates x'_{in} and y_{in} . Equation (22) accounts for all types of aberration that cause either a blur or a lateral shift of the image point and provides a sufficient estimate of the point spread for our investigation. Alternatively, we can treat the lateral shift of the image point as a separate piece of information, calculating the blur of the image point as the sum of the second central moments of the diffraction-limited PSF and the remaining ray aberrations. Depending on the intended application, this may provide an improved estimate of the number of resolved image points.

From the second-order aberrations of the single-lens system we now estimate the SBP. For a given substrate thickness z_D we determine the tilt angle $\vartheta = \vartheta_{\text{opt}}$, which yields the maximum SBP. To calculate ϑ_{opt} , the second moment is determined as the average of the second moments of a set of image points in the image plane. The average spread as a function of ϑ is minimized with a gradient method. To estimate the SBP, the area of the image is finally divided by the mean area of the PSF.

In Figs. 5(a) and 5(b) the optimum angle ϑ_{opt} and the corresponding SBP, respectively, are drawn as a function of z_D . Interestingly, the SBP increases almost linearly with the thickness, contrary to the quadratic increase predicted by paraxial diffraction theory.⁴

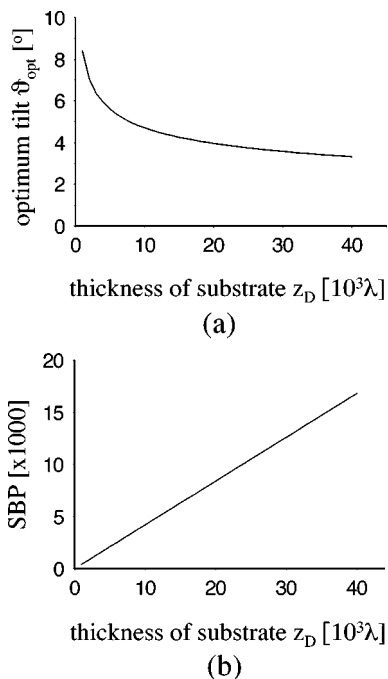


Fig. 5. Imaging performance of the single-lens system: (a) optimum tilt angle of the optical axis, (b) maximum achievable SBP.

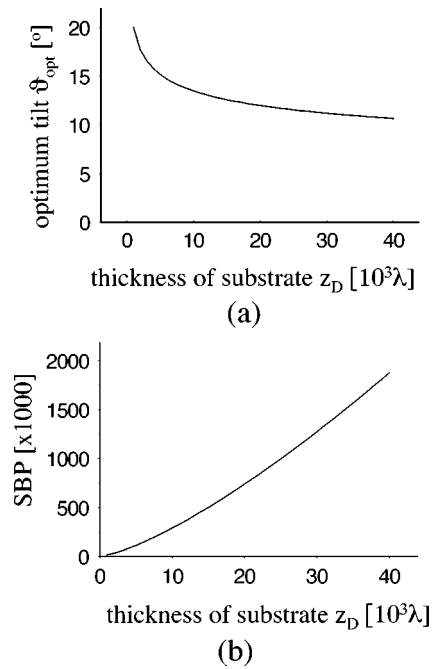


Fig. 6. Imaging performance of the $4f$ system. Plots correspond to those in Fig. 5.

The maximum SBP obtained for the single-lens system is comparatively small. For a substrate of thickness $z_D = 3000\lambda$, the imaging system resolves approximately 35 lines in each direction. This confirms results obtained previously from an analysis of wave aberrations in a single-lens system.⁶ Again, we find that the aberrations caused by the oblique optical axis limit the performance of planar optics significantly, as long as they are not compensated by a more sophisticated design.

The same analysis can be performed for the three-element $4f$ system, assuming perfect correction in the x' direction, as discussed in Section 4. Results for ϑ_{opt} and the SBP are shown in Figs. 6(a) and 6(b). We find a maximum SBP [Fig. 6(b)], which is 2–3 orders of magnitude larger than for the single-lens system. This provides a sufficiently large SBP for most interconnection purposes, even for a moderate substrate thickness. In addition, it leaves enough flexibility to trade the number of channels against the signal-to noise ratio and the inter-channel cross talk.

Comparison of a single-lens system and a $4f$ system clearly indicates the necessity of using a design that is able to compensate for those aberrations introduced by the geometry of planar optics. Furthermore, it demonstrates the large potential that planar-integrated optics offers as an enabling technology for building compact optical interconnects.

Note, however, that the values of the SBP in Figs. 5(b) and 6(b) should be not taken as fixed upper or lower bounds of the imaging capability of planar optics. For instance, the second-order terms of the single-lens system can be traded against higher-order terms to provide an improved performance for a particular imaging task. Similarly, the free parameters of the $4f$ system can be used for further optimization of the SBP rather than for

correction of one spatial coordinate. Our investigation was aimed at pointing out the differences between different planar setups and between conventional optics and planar optics rather than at optimizing a particular imaging system for a specific purpose. For any specific imaging task, additional constraints have to be considered. These include a more careful consideration of channel cross talk and trading of the signal-to-noise ratio against the available SBP. These considerations, however, are beyond the scope of this investigation.

Finally, note the small optimum tilt angles that we found [Figs. 5(a) and 6(a)]. These results are of particular interest, since typically ϑ is chosen to be beyond 10° . From a paraxial analysis of planar systems, it can be shown⁴ that the SBP continuously increases with the tilt angle. Our results indicate, however, that, for imaging systems and other planar systems in which aberrations are competing with diffraction effects, a smaller angle is better suited to resolving a large number of features.

6. CONCLUSIONS

Our investigation of planar optical imaging systems demonstrates that the oblique orientation of the optical axis, which is a common property of planar optics, increases the extent to which aberrations influence the image quality.

The single-lens system serves as a reference to illustrate the changes introduced by the obliquity of the axis: (1) There are aberrations of second order, which do not occur in rotational symmetric systems; and (2) there are third-order aberrations, which cannot be compensated because of the simplicity of the setup.

As with the mirror systems of macro-optics, it is possible to improve the imaging quality by a two- or three-element design. We found the $4f$ system to compensate for most aberrations, including those of all second-order terms. A further reduction of aberrations can be achieved with a proper choice of the lens transmission function. In addition, aberrations can be completely canceled in one coordinate by means of a phase element in the filter plane of the system. The remaining terms allow imaging with a sufficiently large SBP. For both planar systems the comparison of diffraction theory and ray optics, based on the geometrical constraints of planar optics, provides an optimum choice of the free parameters of the planar system.

Our investigation also showed that an optimized design can be obtained for a specific combination of substrate thickness and optical axis tilt. This result is of particular importance, as the tilt angle is typically chosen arbitrarily and is treated as a free parameter. Of similar importance is the small value that we determined for the optimum tilt angle. It is commonly assumed that a large tilt angle is better, since it permits a larger size of the elements, overcompensating the increasing diffraction-limited PSF. Our results indicate, however, that in the presence of aberrations this rule is reversed and that better resolution is obtained for angles smaller than 10° .

For our analysis we used ray tracing of third order based on symbolic computation of ray propagation. This gave us the opportunity to illustrate the properties of pla-

nar optics, keeping the degrees of freedom reasonably small. For practical applications it may be necessary to consider a fifth-order description, which can be obtained directly from the ray-tracing scheme that we used for this investigation. For instance, such a description becomes necessary for small tilt angles ϑ and for problems in which third-order contributions are balanced against fifth-order terms. For planar optics a description of fifth order also includes contributions of fourth order, which must be properly handled.

ACKNOWLEDGMENTS

Helpful discussions with W. Eckert and S. Sinzinger are gratefully acknowledged. This work was financially supported by the Deutsche Forschungsgemeinschaft.

APPENDIX A: ABERRATION COEFFICIENTS OF THE SINGLE-LENS SYSTEM

The appendix summarizes the aberration coefficients of the planar-integrated single-lens system and the $4f$ system described in the text. The deviation of the ray position from the Gaussian image point in the output plane is expressed as the sum of second-order contributions $X_{pq}pq$, $Y_{pq}pq$ and third-order contributions $X_{opq}opq$, $Y_{opq}opq$, where o,p,q can be either x' , v , y or w .

1. Second-Order Coefficients

x coordinate:

$$X_{x'x'} = 2 \frac{\sin \vartheta}{z_D}, \quad X_{x'v} = 4 \tan \vartheta;$$

y coordinate:

$$Y_{x'y} = 2 \frac{\sin \vartheta}{z_D}, \quad Y_{x'w} = 2 \tan \vartheta, \quad Y_{vy} = 2 \tan \vartheta.$$

2. Third-Order Coefficients

x coordinate:

$$\begin{aligned} X_{x'x'x'} &= -\frac{1}{z_D^2} \left(2 - \cos^2 \vartheta - 8 \frac{z_D^3}{\cos \vartheta} a_{2,40} \right), \\ X_{x'x'v} &= -\frac{3}{z_D \cos \vartheta} \left(2 - \cos^2 \vartheta - 16 \frac{z_D^3}{\cos \vartheta} a_{2,40} \right), \\ X_{x'yy} &= -\frac{\cos^2 \vartheta}{z_D^2} \left(1 - 4 \frac{z_D^3}{\cos^3 \vartheta} a_{2,22} \right), \\ X_{x'vw} &= -2 \frac{\cos \vartheta}{z_D} \left(1 - 8 \frac{z_D^3}{\cos^3 \vartheta} a_{2,22} \right), \\ X_{x'vv} &= \frac{1}{\cos^2 \vartheta} \left(2 - 5 \cos^2 \vartheta + 96 \frac{z_D^3}{\cos \vartheta} a_{2,40} \right), \\ X_{x'ww} &= \left(-1 + 16 \frac{z_D^3}{\cos^3 \vartheta} a_{2,22} \right), \\ X_{yyv} &= -\frac{\cos \vartheta}{z_D} \left(1 - 8 \frac{z_D^3}{\cos^3 \vartheta} a_{2,22} \right), \end{aligned}$$

$$X_{yvw} = 2 \left(-1 + 16 \frac{z_D^3}{\cos^3 \vartheta} a_{2,22} \right),$$

$$X_{vvv} = \frac{2z_D}{\cos^3 \vartheta} \left(-3 + 2 \cos^2 \vartheta + 32 \frac{z_D^4}{\cos \vartheta} a_{2,40} \right),$$

$$X_{vww} = \frac{2z_D}{\cos \vartheta} \left(-1 + 16 \frac{z_D^3}{\cos^3 \vartheta} a_{2,22} \right);$$

y coordinate:

$$Y_{x'x'y} = -\frac{1}{z_D^2} \left(2 - 1 \cos^2 \vartheta - 4 \frac{z_D^3}{\cos \vartheta} a_{2,22} \right),$$

$$Y_{x'x'w} = -\frac{1}{z_D \cos \vartheta} \left(2 - \cos^2 \vartheta - 8 \frac{z_D^3}{\cos \vartheta} a_{2,22} \right),$$

$$Y_{x'yy} = -2 \frac{1}{z_D \cos \vartheta} \left(2 - \cos^2 \vartheta - 8 \frac{z_D^3}{\cos \vartheta} a_{2,22} \right),$$

$$Y_{x'vw} = -2 \left(1 - 16 \frac{z_D^3}{\cos^3 \vartheta} a_{2,22} \right),$$

$$Y_{yyy} = -\frac{\cos^2 \vartheta}{z_D^2} \left(1 - 8 \frac{z_D^3}{\cos^3 \vartheta} a_{2,04} \right),$$

$$Y_{yyw} = -3 \frac{\cos \vartheta}{z_D} \left(1 - 16 \frac{z_D^3}{\cos^3 \vartheta} a_{2,04} \right),$$

$$Y_{yvv} = \frac{1}{\cos^2 \vartheta} \left(2 - 3 \cos^2 \vartheta + 16 \frac{z_D^3}{\cos \vartheta} a_{2,22} \right),$$

$$Y_{yww} = -3 \left(1 - 32 \frac{z_D^3}{\cos^3 \vartheta} a_{2,04} \right),$$

$$Y_{vvv} = 2 \frac{z_D}{\cos^3 \vartheta} \left(2 - 3 \cos^2 \vartheta + 16 \frac{z_D^3}{\cos \vartheta} a_{2,22} \right),$$

$$Y_{vww} = -2 \frac{z_D}{\cos \vartheta} \left(1 - 32 \frac{z_D^3}{\cos^3 \vartheta} a_{2,04} \right).$$

APPENDIX B: ABERRATIONS OF THE 4f SYSTEM WITH AN ADDITIONAL PHASE FILTER

The symmetry of the 4f system automatically compensates for all second-order terms. The remaining third-order coefficients are

x coordinate:

$$X_{x'x'v} = 4 \frac{1}{z_D \cos \vartheta} \left(1 - \cos^2 \vartheta + 6 \frac{z_D^3}{\cos \vartheta} a_{1,40} \right),$$

$$X_{x'vw} = 8 \frac{z_D^2}{\cos^2 \vartheta} a_{1,22},$$

$$X_{yyv} = 4 \frac{z_D^2}{\cos^2 \vartheta} a_{1,22},$$

$$X_{vvv} = -\frac{z_D}{\cos^3 \vartheta} \left[2 - \cos^2 \vartheta - 4 \frac{z_D^3}{\cos \vartheta} (2a_{1,40} + a_{2,40}) \right],$$

$$X_{vww} = -\frac{z_D}{\cos \vartheta} \left[1 - 2 \frac{z_D^3}{\cos^3 \vartheta} (2a_{1,22} + a_{2,22}) \right];$$

y coordinate:

$$Y_{x'x'w} = 2 \frac{1}{z_D \cos \vartheta} \left(\sin^2 \vartheta + 2 \frac{z_D^3}{\cos \vartheta} a_{1,22} \right),$$

$$Y_{x'vw} = 2 \frac{1}{z_D \cos \vartheta} \left(\sin^2 \vartheta + 4 \frac{z_D^3}{\cos \vartheta} a_{1,22} \right),$$

$$Y_{yyw} = 24 \frac{z_D^2}{\cos^2 \vartheta} a_{1,04},$$

$$Y_{vvv} = -\frac{z_D}{\cos^3 \vartheta} \left[1 + \sin^2 \vartheta - 2 \frac{z_D^3}{\cos \vartheta} (2a_{1,22} + a_{2,22}) \right],$$

$$Y_{vww} = -\frac{z_D}{\cos \vartheta} \left[1 - 4 \frac{z_D^3}{\cos^3 \vartheta} (2a_{1,04} + a_{2,04}) \right].$$

REFERENCES

1. J. Jahns and A. Huang, "Planar integration of free-space optical components," *Appl. Opt.* **28**, 1602–1605 (1989).
2. J. Jahns, "Integrated optical imaging system," *Appl. Opt.* **29**, 1998 (1990).
3. J. Jahns and S. J. Walker, "Imaging with planar optical systems," *Opt. Commun.* **76**, 313–317 (1990).
4. M. Testorf and J. Jahns, "Paraxial theory of planar integrated systems," *J. Opt. Soc. Am. A* **14**, 1569–1575 (1997).
5. R. Barakat and A. Houston, "The aberrations of non-rotationally symmetric systems and their diffraction effects," *Opt. Acta* **13**, 1–30 (1966).
6. M. Testorf and J. Jahns, "Imaging in planar optics: system design with respect to the angle of light propagation," in *Diffraction Optics and Micro-Optics*, Vol. 5 of 1996 OSA Technical Digest Series (Optical Society of America, Washington, D.C., 1996), pp. 364–367.
7. Ch. Gimkiewicz, D. Hagedorn, J. Jahns, E. B. Kley, and F. Thoma, "Fabrication of microprisms for planar-optical interconnections using analog gray-scale lithography with high-energy beam-sensitive glass," in *Diffraction Optics and Micro-Optics*, Vol. 10 of 1998 OSA Technical Digest Series (Optical Society of America, Washington, D.C., 1998), pp. 175–176.
8. W. Eckert, K.-H. Brenner, and C. Passon, "Planar integration of free-space micro-optical systems with refractive elements," presented at the International Conference on Optical Computing, Edinburgh, August 22–25, 1994.
9. A. Walter, "Eikonal theory and computer algebra," *J. Opt. Soc. Am. A* **13**, 523–531 (1996).

10. C. W. Harris, "Optical design by a matrix method," *J. Opt. Soc. Am.* **40**, 819–822 (1950).
11. J. A. Davis and R. A. Lilly, "Ray-matrix approach for diffractive optics," *Appl. Opt.* **32**, 155–158 (1992).
12. W. T. Welford, "Aberration theory of gratings and grating mountings," in *Progress in Optics*, E. Wolf, ed. (North-Holland, Amsterdam, 1965), Vol. 4, pp. 243–280.
13. G. Schulz, "Primary aberration-free imaging by three refracting surfaces," *J. Opt. Soc. Am.* **70**, 1149–1152 (1980).
14. A. Offner, "New concepts in projection mask aligners," *Opt. Eng.* **14**, 130–132 (1975).
15. W. G. Fastie, "A small plane grating monochromator," *J. Opt. Soc. Am.* **42**, 641–647 (1952).
16. N. Bareket, "Second moment of the diffraction point spread function as an image quality criterion," *J. Opt. Soc. Am.* **69**, 1311–1312 (1979).
17. E. H. Linfoot, "Contrast transmission function at low spatial frequencies," *Opt. Acta* **6**, 387–403 (1959).